AMERICAN JOURNAL OF MATERIALS AND NANOTECHNOLOGY

Zinc Oxide Nanocomposites—Extracellular Synthesis, Physicochemical Characterization and Antibacterial Potential

Paweł Pomastowski [1,*], Anna Król-Górniak [1,2], Viorica Railean-Plugaru [1,2] and Bogusław Buszewski [1,2]

1 Centre for Modern Interdisciplinary Technologies, Nicolaus Copernicus University in Torun, 4 Wilenska´ Str., 87-100 Torun, Poland

2 Department of Environmental Chemistry and Bioanalytics, Faculty of Chemistry, Nicolaus Copernicus University in Torun, 7 Gagarina Str., 87-100 Torun, Poland

Abstract: This research presents, for the first time, the potential of the Lactobacillus paracasei LC20 isolated from sweet whey as a novel, e ective and accessible source for post-cultured ZnO nanocomposites synthesis. The obtained nanocomposites were subjected to comprehensive characterization by a broad spectrum of instrumental techniques. Results of spectroscopic and microscopic analysis confirmed the hexagonal crystalline structure of ZnO in the nanometer size. The dispersion stability of the obtained nanocomposites was determined based on the zeta potential (ZP) measurements—the average ZP value was found to be 29.15 1.05 mV in the 7–9 pH range. The ZnO nanocomposites (NCs) demonstrated thermal stability up to 130 C based on the results of thermogravimetric TGA/DTG) analysis. The organic deposit on the nanoparticle surface was recorded by spectroscopic analysis in the infrared range (FT-IR). Results of the spectrometric study exhibited nanostructure-assisted laser desorption/ionization e ects and also pointed out the presence of organic deposits and, what is more, allowed us to identify the specific amino acids and peptides present on the ZnO NCs surfaces. In this context, mass spectrometry (MS) data confirmed the nano-ZnO formation mechanism. Moreover, fluorescence data showed an increase in fluorescence signal in the presence of nanocomposites designed for potential use as, e.g., biosensors. Despite ZnO NCs' luminescent properties, they can also act as promising antiseptic agents against clinically relevant pathogens. Therefore, a pilot study on the antibacterial activity of biologically synthesized ZnO NCs was carried out against four strains (Escherichia coli, Staphylococcus aureus, Klebsiella pneumoniae and Pseudomonas aeruginosa) by using MIC (minimal inhibitory concentration). Additionally, the colony forming units (CFU) assay was performed and quantified for all bacterial cells as the percentage of viable cells in comparison to a control sample (untreated culture) The nanocomposites were e ective among three pathogens with MIC values in the range of 86.25–172.5 g/mL and showed potential as a new type of, e.g., medical path or ointment formulation.

Keywords: zinc oxide; nanocomposites; extracellular synthesis; Lactobacillus paracasei; organic deposit; antimicrobial activity; mechanism of formation

---

1. Introduction

The production of metal oxide nanomaterials such as zinc oxide nanocomposites (ZnO NCs) is an emerging and currently researched subject in nanotechnology [1,2]. Over the years, synthesis of nanomaterials has been of research interest but there is a growing need for development of more e cient, facile and environmentally friendly methods. Therefore, synthesis of nano-ZnO using biological systems is attracting rising attention, mainly due to the lower consumption of hazardous reagents and lower cytotoxicity of the obtained nanomaterials (in comparison with traditional chemical and physical methods). Biosynthesis of zinc oxide can be carried out with various biological materials including bacteria, fungi and plant extracts [3–5]. There is limited evidence of e ective ZnO nanoparticle formation using plants, whereas the adoption of a microbiological approach for this purpose has still not been su ciently described. Among methods of microbial synthesis, two main types can be identified—intra- and extracellular methods. Intracellular production involves bacteria biomass for the nanocomposite formation, while the extracellular approach, known also as the post-cultured method, excludes microbial cells and uses a supernatant rich in biologically active compounds (e.g., enzymes or metabolites) [6]. As has been highlighted by literature data [7–9], the post-cultured method (extracellular synthesis) has its advantages, such as lower cost, simpler downstream processing (e.g., nanomaterial separation and purification processes) and possibility to reuse the bacterial cultures. Moreover, the extracellular approach is also a more adequate choice to produce nanocomposites with organic deposits on their surfaces coming from microbial compounds of natural origin. Railean-Plugaru et al. [10] obtained bio-AgNCs with the specific organic deposit connected with the silver core of nanoparticles. According to the latest literature data, there is no paper describing ZnO NCs synthesized by lactic acid bacteria (LAB) strain, naturally coated by organic deposit.

Despite the type of nanomaterial synthesis, it is necessary to consider the parameters such as selection of the organisms, as well as the precursor salts, that are the most suitable for this purpose and the type of synthesis. Kalpana et al. [4] used cell filtrates of Aspergillus niger to perform ZnO NP production. The nanomaterial obtained in this work revealed antimicrobial activity and showed the potential for dye degradation. Another example is the work of Kundu et al. [11], who performed the synthesis of ZnO nanoparticles by using cell-free filtrate after Rhodococcus pyridinivorans NT2 culturing and zinc sulfate as a precursor. They underlined the critical role of extracellular bioactive compounds of the strain (e.g., proteins) in the formation and stabilization of nano-ZnO.

LABs exhibit beneficial effects on humans—they colonize the digestive system involved in normal digestive processes (microflora) or act as a protective barrier on the skin's surface. Moreover, their metabolites are generally regarded as safe and exhibit antimicrobial activity [12,13]. However, there are only a few reports describing the e cient and intracellular synthesis of nano-ZnO by using lactic acid bacteria biomass [14–16]. The lack of papers related to the post-cultured ZnO NP formation method with LAB metabolites has forced scientists to develop a novel, e cient and simple synthesis protocol. Designing metal nanocomposites based on biologically active and accessible LAB metabolites provides an opportunity to reduce or even inhibit a pathogen's growth. Currently, antibiotic resistance among pathogenic bacteria is a real problem for humanity [17–19]. The increasing problem of drug-resistance among many pathogens, e.g., Staphylococcus aureus, Pseudomonas aeruginosa, Klebsiella pneumonia or Escherichia coli, requires the development of novel antiseptics [20–23]. One of the prospective alternatives to antibiotics is, as proposed in our study, the post-cultured synthesis of zinc oxide nanocomposites by lactic acid bacteria isolated from whey. The use of these natural raw materials as a source of a specific "bioreactor" capable of forming ZnO NCs perfectly fits in with the idea of environmental protection and sustainable development. Furthermore, using probiotic strains for nano-ZnO synthesis allows the formation of nanomaterials with specific organic deposits on their surfaces coming from microorganisms' cells.

In our study, the probiotic strain (Lactobacillus paracasei LC20) isolated from sweet whey was chosen for the production of ZnO nanocomposites. Although whey is the subject of much controversy, because it can pose a risk to the environment if is not properly managed, it is, on the other hand, a rich source of valuable compounds (e.g., proteins, vitamins) and lactic acid bacteria (LAB) [24,25]. Due to the rich composition of whey, it is very important to find new, easy and environmental friendly technology not only for the utilization of this product but also for using it as a precious raw material.

Therefore, the main aim of this work was to carry out post-cultured ZnO nanocomposite synthesis by Lactobacillus paracasei LC20 isolated from sweet whey. The use of whey in the role of natural raw material creates new possibilities to apply it as a novel and eco-friendly source of LAB strains and, consequently, for the nano-ZnO. The obtained ZnO NCs were physicochemically characterized by di erent instrumental techniques. Based on the spectroscopic (FT-IR) and spectrometric (LDI-MS, spectrofluorimetry) experimental data, the presence of specific organic deposits on the ZnO NCs' surfaces, together with the improvement of the fluorescence in the presence of ZnO NCs, was demonstrated. The antibacterial properties of biologically synthesized nanocomposites were investigated against both Gram(+) and Gram( ) drug-resistant bacteria strains by determining the MIC value (86.25–172.5 g/mL) which indicates the antiseptic ZnO NC activity among relevant pathogens. The described unique attributes (organic surface deposits or luminescence properties) of bio-synthesized ZnO nanocomposites indicate the potential for their further application in both medicine and engineering fields. Finally, the results of MS analysis also support the previous description of ZnO NCs' formation mechanism.

2. Materials and Methods

2.1. Isolation and Identification of Bacterial Strain

The probiotic strain was isolated from sweet whey at pH > 6 (Dairy Cooperative in Drzycim, Poland) according to the previous protocol [26]. The molecular identification of bacterial strain was performed by MALDI-TOF-MS identification by the ultrafleXtreme mass spectrometer (Bruker Daltonics, Hamburg, Germany) using formic acid-acetonitrile extraction and BioTyper identification [26]. Finally, the isolated strains of L. paracasei LPC20 were deposited in the Polish Collection of Microorganisms (PCM) under deposit no. B/00287.

2.2. Extracellular Synthesis of Zinc Oxide Nanocomposites (ZnO NCs)

For the extracellular synthesis of ZnO NCs, the Lactobacillus paracasei LPC20, from the collection of Centre for Modern Interdisciplinary Technologies, Nicolaus Copernicus University in Torun,´ isolated from sweet whey (Dairy Cooperative in Drzycim, Drzycim, Poland) [27], was chosen. The L. paracasei LPC20 strain was grown on Müller–Hinton broth (MH, Sigma-Aldrich, St. Louis, MO, USA) and incubated at 37 C for 24 h. After the incubation, the culture was centrifuged at 12,000 rpm for 30 min and the cell-free supernatant was collected and used for further ZnO NC synthesis. As a precursor of ZnO, zinc nitrate ($Zn(NO_3)_2$) at 0.1 g/mL concentration was chosen and added to the supernatant under continuous magnetic stirring. Then, the synthesis was carried out at 60 C for 1 h. After this time, the mixture was centrifuged (7000 rpm, 15 min) and the obtained supernatant was transferred to a new container and heated at 100 C until a dried precipitate appeared. The collected ZnO powder was washed with distilled water three times. Then, unbounded ions as well as low molecular weight metabolites were removed by 5-day dialysis (3 kDa cuto , Spectrum Lab, Thermo Fisher Scientific, Vantaa, Finland). As a control, MH broth instead of L. paracasei LCP20 supernatant was used.

2.3. Physicochemical Characterization of ZnO NCs

2.3.1. Zeta Potential Measurement

The ZnO NC zeta potential value was determined with Zetasizer Nano Series (Malvern Instruments, Malvern, Great Britain). Before measurement, the ZnO NCs (at 0.05 mg/mL concentration) were suspended in water at specific pH (range of 2 to 11) and mixed for 5 min. The measurements included three repetitions for each sample. The zeta potential data obtained were processed using Curve Expert Professional 2.6.5 software (Hyams Development, Huntsville, AL, USA). According to the electrokinetic theory, the processed data were fitted to the rational model. All measurements were carried out in triplicate.

2.3.2. Fourier Transform Infrared Spectroscopy Analysis

Concerning the active functional groups present on ZnO NCs, FT-IR analysis was performed using a Spectrum 2000 (Perkin-Elmer, Waltham, MA, USA) in the range of = 400–4000 cm ^{1}. The sample was prepared by application of the KBr disc method. The spectroscopic data were processed with OPUS 7.5 software (Bruker Daltonics, Hamburg, Germany).

2.3.3. Transmission Electron Microscopy (TEM) and Energy Dispersive X-ray (EDX) Analysis

The structure and surface morphology of the obtained ZnO NCs were investigated by scanning electron microscopy with focused ion beam (SEM/FIB—Quanta 3D FEG, FEI, Gräfelfing, Germany). The confirmation of ZnO nanoparticles' presence in nanoscale was examined by transmission electron microscopy (TEM, FEI Tecnai F20 X-Twin, Hillsboro, OR, USA) coupled with energy dispersive X-ray (EDX) detector (RTEM SN9577, 134 eV, Edax, Mahwah, NJ, USA). For SEM analysis, ZnO NC powder was used, whereas for transmission electron microscopy investigation, sample solution was put on a carbon-coated grid and the excess solution was removed.

2.3.4. Spectrofluorometric Analysis

The ZnO NCs were analyzed with a JASCO FP-8300 spectrofluorometer (JASCO Europe, Cremella, Italy) and the three-dimensional (3D) excitations and emission spectra were recorded with 5 nm wavelength interval in the 210–735 nm range. As a control sample, zinc nitrate and water were used.

2.3.5. X-ray Di raction Study

In order to characterize the crystalline structure of the obtained ZnO NCs, the X'Pert Pro Analytical di ractometer (Phillips, Erlangen, Germany) equipped with CuK (= 1.54056 Å) radiation source and Ni filter was used. The powder sample was analyzed and the crystallite size of sample was calculated based on the Scherrer equation [28]. The registered XRD pattern was processed using XRD Malvern Panalytical software (version 1.5a (1.5.1.135), Almelo, The Netherlands). As a control sample, MH broth instead of L. paracasei LCP20 supernatant as well as the chemically obtained ZnO NCs were used.

2.3.6. Thermogravimetric Analysis (TG-DTA)

Thermal analysis of the obtained nanomaterial was performed by using TA Instruments type SDT
2960 (Artisan Technology, Champaign, IL, USA) in the range of 0–1000 C with an air flow rate of 100 mL/min and heating rate of 10 C/min. All data were processed by TGA-DTA thermal analysis

software (version V5 7.0, TA Instruments, New Castle, DE, USA). All measurements were carried out in triplicate.

2.3.7. Laser Desorption/Ionization with Mass Spectrometry Analysis (LDI-TOF-MS)

The LDI-TOF-MS analysis was performed using ultrafleXtreme mass spectrometer (Bruker Daltonics, Hamburg, Germany) and ZnO NCs suspended in water were spotted on the ground steel target (Bruker Daltonik, Bremen, Germany) according to the previously described protocol [10] with the required modification (without the -Cyano-4-hydroxycinnamic acid (HCCA) matrix). Protein Calibration Standards I (Bruker Daltoniks, Bremen, Germany), Peptide Calibration Standard and two signals characteristic for the matrix $[M-H]^+$ and $[2M-H]^+$ were used for the external calibration, according to the standardized Bruker sample preparation procedure. Molecular fingerprint (MF) spectra of ZnO NCs were recorded in reflectron positive mode, within a m/z range of 100–3500, and we applied an acceleration voltage of 25 kV. Fragment spectra were recorded using the LIFT default method (Bruker Daltonics, Hamburg, Germany) at 100% of laser power, global attenuator 50% with calibration on the immonium ions [29,30]. The voltage on the LIFT electrodes was 19.0 and 2.7 kV, respectively. MS spectra were registered in FlexControl (Bruker Daltonics, Hamburg, Germany), while the FlexAnalysis (Bruker Daltonics, Hamburg, Germany) was used for data analysis.

2.4. Antimicrobial Potential of ZnO NCs

Colony Forming Unit (CFU) and Minimal Inhibitory Concentration (MIC)

Four different relevant microorganisms such as Staphylococcus aureus ATCC 11632, Pseudomonas aeruginosa ATCC 15441, Klebsiella pneumoniae ATCC BAA-1144 and Escherichia coli ATCC 25922, received from the Pol-Aura company (Pol-Aura, Olsztyn, Poland), were chosen for the antimicrobial activity of extracellularly synthesized ZnO NC determination. All chosen bacterial strains were revived in Mueller–Hinton (MH) broth to 1 10^6 CFU/mL. The concentration of ZnO NCs was determined by inductively coupled plasma mass spectrometry (ICP-MS) analysis and dilutions of ZnO NCs were prepared (172.5, 86.25, 43.125, 21.56, 10.78, 5.39, 2.69 and 1.35 g/mL, respectively). The growth bacterial cells (1 10^6 CFU/mL) were mixed with the prepared concentration in the ratio 1:1. To the prepared mixture, 12 L of in vitro toxicology assay kit, resazurin based (Sigma-Aldrich, St. Louis, MO, USA) was added. After 24 h of incubation at 37 C, the MIC value was determined visually based on the change in the redox indicator color from blue to pink or colorless. The lowest concentration at which no change in color was observed was considered as the MIC value, according to [31]. All the experiments were prepared in triplicate.

Additionally, all the bacteria were subjected to the colony forming unit (CFU) assay. To determine the sensitivity of bacterial strains to biologically synthesized ZnO NCs, bacteria were grown in the presence of nanocomposites (at concentrations of 345, 172.5 and 86.25 g/mL, respectively) at 37 C for 24 h. After the incubation, various dilutions (10 ^{1}–10 ^{8} folds) of bacterial suspension were prepared. Then, 100 L of each sample was transferred to tryptic soy agar TSA plates, incubated at 37 C for 24 h, and CFU were counted manually. NC-free bacteria strains were used as a negative control while ampicillin at 10 g/mL concentration for S. aureus, E.coli and K. pneumoniae, and at 25 g/mL concentration for P. aureginosa, was used as a positive control. The CFU assay was performed in triplicate. The concentration of ZnO NCs was estimated from the observed MIC values for each bacterial strain and the concentration of ampicillin was based on the European Committee on Antimicrobial Susceptibility Testing (EUCAST) breakpoints table.

3. Results and Discussion

The synthesis of ZnO nanomaterials can be carried out by using various types of biological sources such as proteins, plant extracts or microorganisms. Recent studies have demonstrated that both intra-and extracellular approaches are e cient enough to synthesize di erent types of nanoparticles, e.g., silver [10,27,32], gold [33] or titanium oxide [34] NPs; however, the microbial synthesis of nan-ZnO has still not been su ciently described.

3.1. Physicochemical Characterization of ZnO NCs

Figure 1A (SEM image) shows the homogenous structure of the biologically synthesized ZnO NCs. The TEM image of bio-ZnO NCs with the EDX spectra are shown in Figure 1B,C and indicate the presence of zinc (with approximately 1, 8.5 and 9.5 keV signals) and oxide as a major element in the sample [35]. Theoretically, the expected stoichiometric mass percent of oxygen and zinc is 19.7% and 80.3%, respectively. According to the EDX analysis (Figure 1C), the weight percentage of Zn and O in our sample was 19.46% and 80.53%, which is in with good correlation with the theoretical values [36]. Slight di erences observed between the experimental and hypothetical data can be assigned to the presence of some organic deposits coming from the bacterial metabolites or proteins secreted by the bacterial strains during the inoculation step. Moreover, on the EDX spectra, the signal of copper is present—it corresponds to the TEM grid.

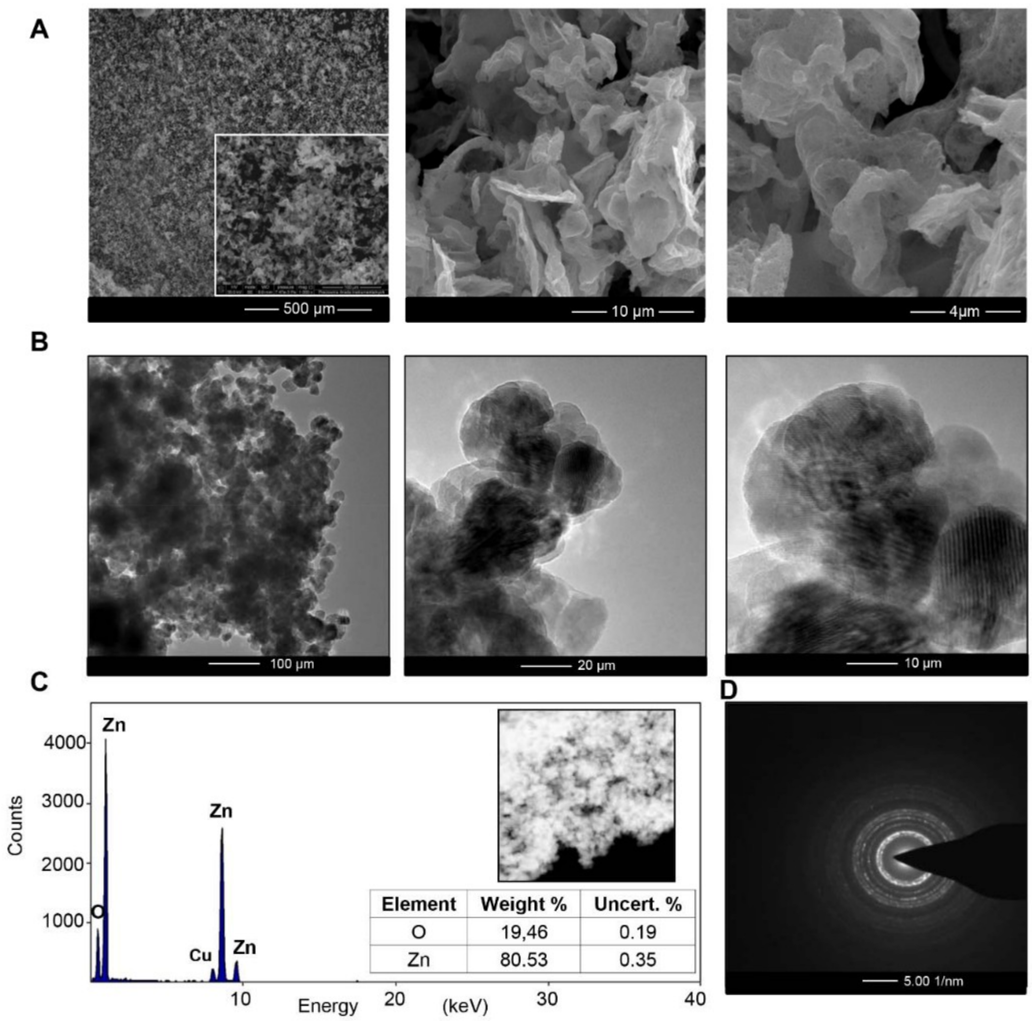

FigureFigure1.SEM**1.**SEMmicrographmicrograph(**A**),(**A**TEM),TEMmicrograph ((**B**), EDX spectra(**C**(**C**)and)andselectedselectedareaarea(electron)(electron)
di raction (SAED)(SAED) of biologically synthesized ZnO NCs.
diffraction (**D**) of biologically synthesized ZnO NCs.

The selected area of diffraction pattern (SAED) (Figure 1D) confirmed the highly crystalline The selected area of di raction pattern (SAED) (Figure 1D) confirmed the highly crystalline nature

nature of the synthesized nanoparticles, which is strongly related to the pattern obtained during XRD

of the synthesized nanoparticles, which is strongly related to the pattern obtained during XRD analysis analysis (Figure 2). Typical ZnO peaks present at 2θ = 31.93°, 34.59°, 36.41°, 47.7°, 56.75°, 63.02° and

(Figure 2). Typical ZnO peaks present at 2 = 31.93 , 34.59 , 36.41 , 47.7 , 56.75 , 63.02 and 68.09 68.09° correspond to the Bragg reflections identified as (100), (002), (101), (102), (110), (103), (200), correspond to the Bragg reflections identified as (100), (002), (101), (102), (110), (103), (200), (112) and (112) and (201), respectively. Data from the XRD analysis clearly illustrate the formation of the

(201), respectively. Data from the XRD analysis clearly illustrate the formation of the wurtzite structure wurtzite structure of zinc oxide (according to the Joint Committee on Powder Diffraction Standard

of zinc(JCPDS)oxide card(according no.36-1451,tothe P63mc)Joint at Committee the 13.70± 1on.53 Powder nmsize

(calculated Diraction from Standard theScherrer(JCPDS) equation card no. 36-1451,

[28])P63mc).InFigureatthe2C,13one.70additional1.53nmpeaksizearound(calculated25°wasfromdete

ctedtheScherrer—itmightequationbeassigned[28]).toIntheFigurezinc 2C, one

additionalhydroxynitratepeak(JCPDSaroundNo:2572-0627)was . detectedAccording—toit

themightliteraturebeassigneddata[37–to39],thezinczincnitratehydroxynitrateZn(NO3)2

(JCPDSor No:itshydroxides72-0627). isAccordingoneofthe tointermediatetheliteratureproductsdata [of37ZnO–39],NCzincsynthesisnitrate. Zn(NOOntheother$_3$)$_2$orhand,itshydroxidesinthe control sample (Figure 2C), no zinc oxide was formed, which indicates that only the specific

is one of the intermediate products of ZnO NC synthesis. On the other hand, in the control sample combination of biologically active compounds from supernatant allows for effective ZnO NC (Figure 2C), no zinc oxide was formed, which indicates that only the specific combination of biologically formation. The difference between the ZnO NCs' size estimated from the TEM and XRD analysis can

active compounds from supernatant allows for e ective ZnO NC formation. The di erence between be attributed to the fact that the particles are formed from more than one crystallite [40,41]. the ZnO NCs' size estimated from the TEM and XRD analysis can be attributed to the fact that the Furthermore, nanoparticles tend very often to create aggregates—therefore, the proper sample particles are formed from more than one crystallite [40,41]. Furthermore, nanoparticles tend very often to create aggregates—therefore, the proper sample preparation steps are decisive [2]. In the case of the control sample, no zinc oxide was detected (Figure 2).

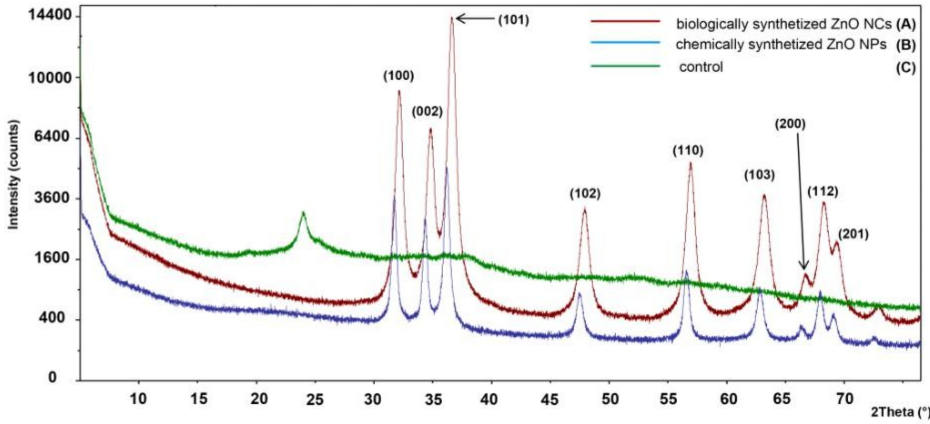

Figure 2. XRD pattern of biologically synthesized (**A**), reference ZnO NCs (**B**) and control (**C**).
Figure 2. XRD pattern of biologically synthesized (**A**), reference ZnO NCs (**B**) and control (**C**).

The presence of organic deposits on the ZnO NCs' surfaces was studied by both spectroscopic (FT-IR) (Figure 3) and spectrometric (LDI-MS) (Figure 4) techniques. Fourier-transform infrared spectroscopy proved the presence of functional groups which contributed to the process of nano-ZnO formation, while mass spectrometry is useful technique for the analysis of metal/metal oxide nanomaterials with organic deposits, mainly due to the isotopic pattern of d-electron metals [42].

Figure 3 represents the biologically synthesized ZnO NC spectra in the mid-infrared (MIR) range. A signal at υ = 1587–1592 cm^{-1} (1) is associated with the NH_2 scissoring vibration of phenylalanine (Phe) amino acid, whereas the vibration at υ = 1695 cm^{-1} is related to the Phe carboxylic acid (C = O stretching) [43,44]. The signal localized at υ = 1648–1685 cm^{-1} (1) is often characteristic of leucine (Leu) $_{as}NH_3^+$ side chain vibration [45,46]. Moreover, the change in the IR spectrum at 1560 cm^{-1} (1) is a result of the deprotonated carboxyl (COO^-) group of glutamic and aspartic acids (Glu and Asp, respectively) [37,38,47]. In the ZnO NC FT-IR spectra, a signal at υ = 1400 cm^{-1} (2) was observed—it is correlated with the plane bending of methylene ($-CH_2$) in the cysteine (Cys) or glycine amino acids [48,49]. In the range of 1100–1200 cm^{-1} (3), there is an area of C-C stretching: C-H and N-H bending vibrations are typical for amide III [44,46,50,51] but also for lactic acid and its metabolites [52]. Additionally, the signal at υ = 800–900 cm^{-1} (4) is related to the C-H vibrations of bioactive compounds included in the organic deposit on the ZnO NC surface (such as peptides or lipids) [10,47,52]. The band at υ = 730–770 cm^{-1} (5) corresponds to the aromatic amino acids side chains (e.g., in the phenylalanine) [43]. The FT-IR spectra (Figure 3) also confirmed the presence of zinc oxide formation—the peak at the region between 500 and 600 cm^{-1} (6) is related to the Zn-O bond [2,53].

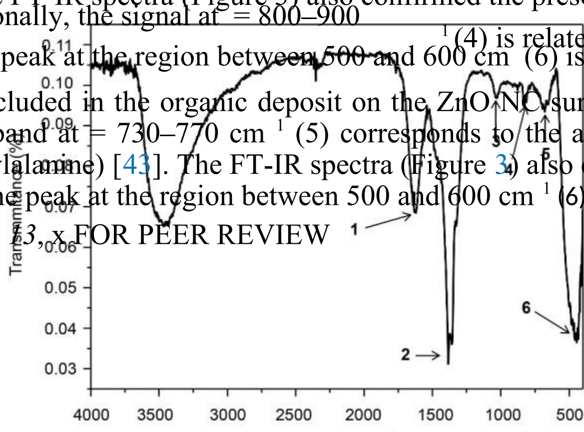

Figure 3. FT-IR spectra for biologically synthesized ZnO NCs in the υ = 400–4000 cm^{-1} range; υ (cm^{-1}): 1: 1600–1700, 2: 1400, 3: 1100–1200, 4: 800–900, 5: 700–800, 6: 500–600.

1: 1600–1700, 2: 1400, 3: 1100–1200, 4: 800–900, 5: 700–800, 6: 500–600.

The recorded molecular fingerprint of ZnO NC nanostructure-assisted laser desorption/ionization is shown in Figure 4A,B,E and presents the MS/MS analysis in LIFT mode of the 606.129, 625.113, 942.233 and 1035.295 *m*/*z* signals, respectively. The signal at 606.129 *m*/*z* (Figure 4C) was assigned to the ionized fragment of three amino acid (Cys, Gly and Asn) peptides with the bounds of 2 Zn2+ and 10 H2O molecules. Another is two Zn2+ bound to the fragments of three amino acids—phenylalanine, aspartic acid and isoleucine (625.113 *m/z*; Figure 4D). These two signals are

The recorded molecular fingerprint of ZnO NC nanostructure-assisted laser desorption/ionization is shown in Figure 4A,B,E and presents the MS/MS analysis in LIFT mode of the 606.129, 625.113, 942.233 and 1035.295 m/z signals, respectively. The signal at 606.129 m/z (Figure 4C) was assigned to the ionized fragment of three amino acid (Cys, Gly and Asn) peptides with the bounds of 2 Zn^{2+} and 10 H_2O molecules. Another is two Zn^{2+} bound to the fragments of three amino acids—phenylalanine, aspartic acid and isoleucine (625.113 m/z; Figure 4D). These two signals are linked with the water. LDI MS/MS measurements also showed the presence of a signal at 942.233 m/z $[Zn_5\text{-}(H_2O)_{28}\text{-}Asn]^+$ and 1035 m/z $[Zn_5\text{-}(H_2O)_{23}\text{-}iAsp\text{-}iGlu\text{-}iCys]^+$ signals (Figure 4F,G). What is interesting, between them, is that five molecules of water were found. The obtained results confirm the presence of organic deposits in the ZnO NC structure which is correlated with the FT-IR data. Moreover, the type of amino acid interacting with the zinc ions and the presence of water molecules is strongly associated with the previously described mechanism of ZnO NC formation [5,54]. The ability of metal ions to bind the specific protein functional groups is highly connected to Me^{2+} nature. Zinc, with its unique coordination chemistry, forms stable aqua complexes, $[Zn(H_2O)_6]^{2+}$, which are able to exchange their water molecules when binding to other ligands, mainly nitrogen ones [55]. Many literature reports have demonstrated that Zn^{2+} bind preferentially to the proteins through negatively charged (aspartic and glutamic acids; Asp and Glu , respectively) or polar residues (cysteine, histidine and asparagine) [56–58]. Molecular dynamics (MD) and density functional theory (DFT) calculations performed by our research group (not published yet) have indicated that the proton transfer reaction results in the formation of an aqua-hydroxo complex $[Zn(OH)(H_2O)_5]^+$. Then, it can be transformed to zinc oxide, through $[Zn(OH)_4]^2$ and $Zn(OH)_2$. Therefore, the presented data confirmed the possible formation of Zn^{2+} (as an aqua complex) during biosynthesis and the mechanism of ZnO NC formation (Figure 5). To sum up, the MS/MS analysis confirm the data from the FTIR and point out the specific peptide fragments taking part in ZnO NC formation.

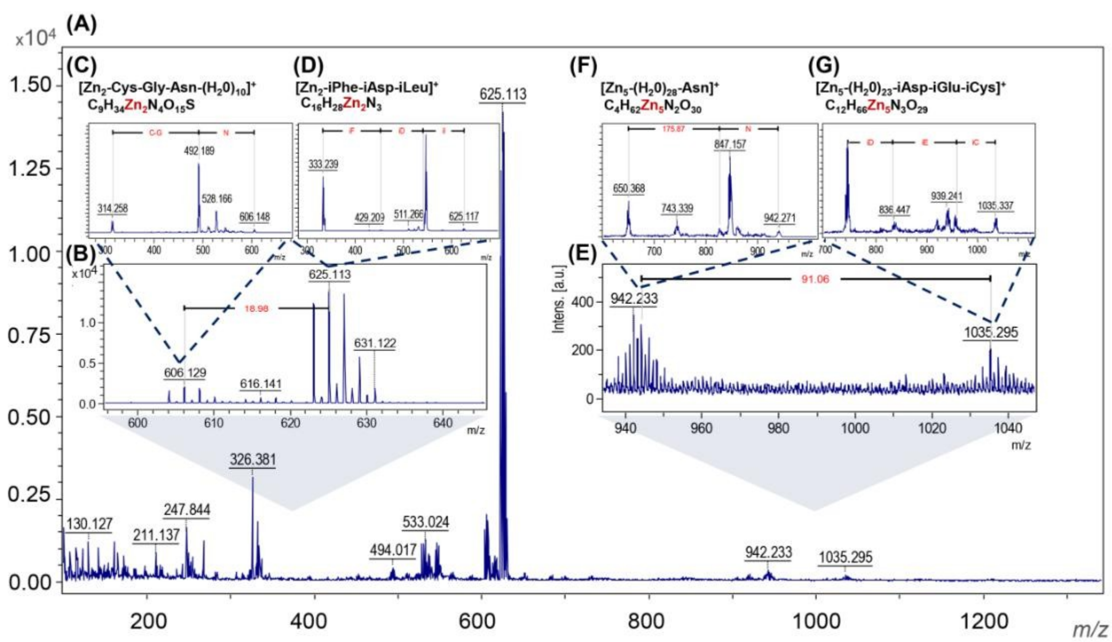

Figure 4. The molecular fingerprintfingerprint of biologically synthesized ZnO NCs (**A**); the MS/MS spectra for specificspecific signals (**B**–**G**)..

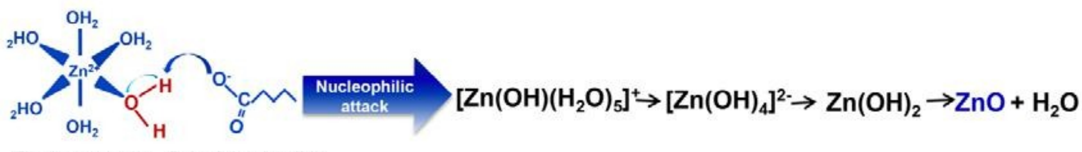

Figure 5. The proposed mechanism of ZnO NC formation.

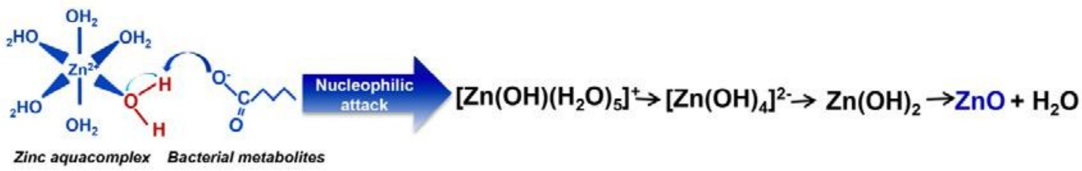

Figure 5. The proposed mechanism of ZnO NC formation.

As a complementary analysis, the 3D spectrofluorometric profiles of biologically synthesized As a complementary analysis, the 3D spectrofluorometric profiles of biologically synthesized ZnO NCs, water and zinc nitrate (as a control) were recorded (Figure 6). In the case of the obtained ZnO NCs, water and zinc nitrate (as a control) were recorded (Figure 6). In the case of the obtained nanocomposites (Figure 6C), the excitation and emission wavelengths were found to be 270, 295 nm (I); nanocomposites (Figure 6C), the excitation and emission wavelengths were found to be 270, 295 nm 250, 510 nm (II), 455, 465 nm (III) and 265, 390 nm (IV), respectively. Band no. IV is characteristic of (I); 250, 510 nm (II), 455, 465 nm (III) and 265, 390 nm (IV), respectively. Band no. IV is characteristic the zinc oxide optical band gap [11,54,59] while band no. III might be correlated with the presence of of the zinc oxide optical band gap [11,54,59] while band no. III might be correlated with the presence organic deposits in the ZnO NC structure. In comparison to the control samples, the presence of the of organic deposits in the ZnO NC structure. In comparison to the control samples, the presence of biologically synthesized nano-ZnO generated an increase in quartz fluorescence intensity (band II)—it the biologically synthesized nano- ZnO generated an increase in quartz fluorescence intensity (band is strongly related with the surface plasmon resonance (SPR) e ect [60]. Surface plasmon resonance II)—it is strongly related with the surface plasmon resonance (SPR) effect [60]. Surface plasmon occurs as a resonance e ect due to the interaction of nanoparticle conduction electrons with incident resonance occurs as a resonance effect due to the interaction of nanoparticle conduction electrons photons [61]. This interaction is related to a large enhancement of the field intensity and, consequently, with incident photons [61]. This interaction is related to a large enhancement of the field intensity with the enhancement of the fluorescence signal [60,62,63]. A similar e ect was presented by many and, consequently, with the enhancement of the fluorescence signal [60,62,63]. A similar effect was researchers [5,10,54,62] as well as in our previous work [54]—the addition of synthesized ZnO NCs presented by many researchers [5,10,54,62]] as well as in our previous work [54]—the addition of enabled an improvement in the intensity of fluorescence emission. The consequences of the observed synthesized ZnO NCs enabled an improvement in the intensity of fluorescence emission. The surface plasmon resonance, such as the increase in the fluorescence signal, create new application consequences of the observed surface plasmon resonance, such as the increase in the fluorescence possibilities for biologically synthesized ZnO NCs, e.g., as biosensors in medical diagnostics. Currently, signal, create new application possibilities for biologically synthesized ZnO NCs, e.g., as biosensors analytical chemistry is based, more and more, on modern instruments, and scientists have at their in medical diagnostics. Currently, analytical chemistry is based, more and more, on modern disposal a wide range of di erent analytical methods. Almost every week, new papers, works and instruments, and scientists have at their disposal a wide range of different analytical methods. Almost the development of new approaches are presented. Many of them are used not only in the chemistry every week, new papers, works and the development of new approaches are presented. Many of field but also in biological and nanotechnology sciences or in medicine as well. Among others, them are used not only in the chemistry field but also in biological and nanotechnology sciences or NALDI-TOF/MS (nonporous-assisted laser desorption/ionization time-of flight mass spectrometry) in medicine as well. Among others, NALDI- TOF/MS (nonporous-assisted laser desorption/ionization is arousing a lot of interest. It is a matrix-free soft laser base MS technology mainly used for low time-of flight mass spectrometry) is arousing a lot of interest. It is a matrix-free soft laser base MS molecular weight biomolecules and organic molecules and classified as the new generation of mass

technology*Materials* **2020**mainly,*13,x* usedFORPEERforREVIEWlowmolecular weight biomolecules and organic molecules and10classifiedof18 spectrometry [64,65]. Previous studies have indicated that an inorganic matrix with large surface area, as the new generation of mass spectrometry [64,65]. Previous studies have indicated that an inorganic

matrix with large surface area, high photon absorption efficiency and low heat capacity is suitable high photon absorption ciency and low heat capacity is suitable for realizing e ective desorption and for realizing effective desorption and ionization. According to this information, nano-ZnO, as a semi-ionization. According to this information, nano-ZnO, as a semi-conductive material, can absorb energy

conductive material, can absorb energy from the laser in wavelengths typically used in MALDI and from the laser in wavelengths typically used in MALDI and transfer it to the analyte [64]. Watanabe et

transfer it to the analyte [64]. Watanabe et al. [66] have used ZnO nanoparticles for the al. [66] have used ZnO nanoparticles for the desorption/ionization of several small molecules, which is

desorption/ionization of several small molecules, which is still an analytical challenge. Kang et al. still an analytical challenge. Kang et al. [64] compared a suspension of analyte/ZnO nanowires and the

[64] compared a suspension of analyte/ZnO nanowires and the direct deposition of the analyte onto

directthedepositionsurfaceof ofananowiretheanalytechiponto.Takingthe thissurfaceinto consideration,ofnanowirethechipresults.Takingofourthisstudyintohaveconsideration,shown the

resultsthatbiologicallyfourstudysynthesizedaveshownZnONCsthatseembiologicallytobepromisingsynthesizedmatrixZn Ofor NCsLDIexperimentsseemtobe since,apromising matrixthisforwork,LDI theexperimentsMALDIanalysissince, inwasthisperformedwork,thewithoutMALDIanyanalysismatrix. was performed without any matrix.

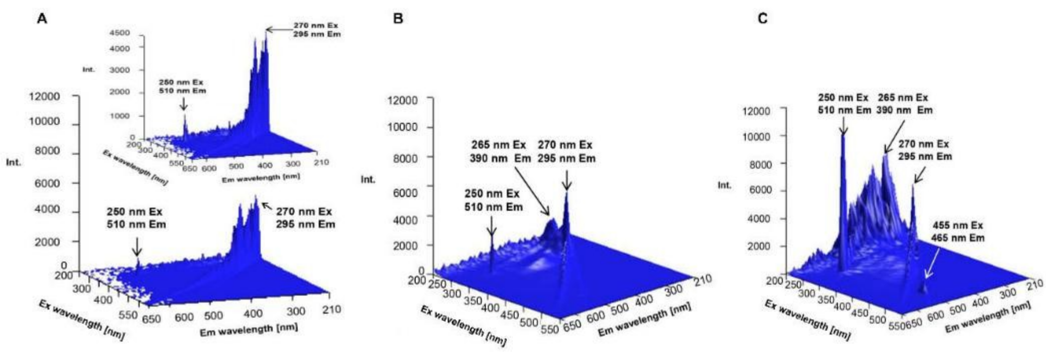

FigureFigure6. Fluoresc**6.e**scencespectraofofwater(**A**(**A**),), zi**nc** **n**itrate(**B**(**B**),),biologicallys**y**synthesizedZnOZnONCs **NCs**(). (**C**).

The stability of the obtained nanomaterials was estimated by the zeta potential measurement. According to the electrokinetic theory and Smoluchowski equation, biocolloids have a surface charge that attracts a thin layer of ions of the opposite charge to the nanoparticle surface. Consequently, the electric potential at the boundary of the double layer is called the zeta potential of the NCs. In our study, in a range of pH 2–6, the biologically synthesized ZnO NCs are unstable and might create

The stability of the obtained nanomaterials was estimated by the zeta potential measurement. According to the electrokinetic theory and Smoluchowski equation, biocolloids have a surface charge that attracts a thin layer of ions of the opposite charge to the nanoparticle surface. Consequently, the electric potential at the boundary of the double layer is called the zeta potential of the NCs. In our study, in a range of pH 2–6, the biologically synthesized ZnO NCs are unstable and might create some aggregates—their zeta potential value varied from 12.63 0.66 to 22.01 0.59 mV (Figure 7A). Instability of the system in this pH scope is associated with the deprotonation of organic deposits (such as carboxyl groups on the NC's surface) [32]. Above pH 6, the zeta potential (ZP) value slightly decreased, and at pH 7–9, the average ZP value at 29.15 1.05 mV clearly indicated that ZnO nanocomposites are fairly stable. Taking into consideration the literature data, the ZP value of NCs formed in our study is higher than the zeta potential of ZnO NPs synthesized intracellularly with L. plantarum (15.3 mV) [14], L. paracasei LB3 (16.2 mV) [54], as well as those obtained during extracellular synthesis by using R. pyridinivorans (15.5 mV) [11]. Above pH 9, the ZP value was higher again (22.57 1.15 mV) and the system was unstable. This phenomenon can be interpreted as the transformation of colloidal $Zn(OH)_{2(S)}$ to $Zn(OH)_{2(aq)}$ ions in the alkaline pH region [67]. In neutral aqueous conditions, the $Zn^{2+}{}_{(aq)}$ and $Zn(OH)^{+}{}_{(aq)}$ ions are in equilibrium with surface hydroxide, while at higher pH, the dominant species are $Zn(OH)_{2(aq)}$, which are able to precipitate and create aggregates. In consequence, the stability of nano-ZnO is definitely lower [67–69].

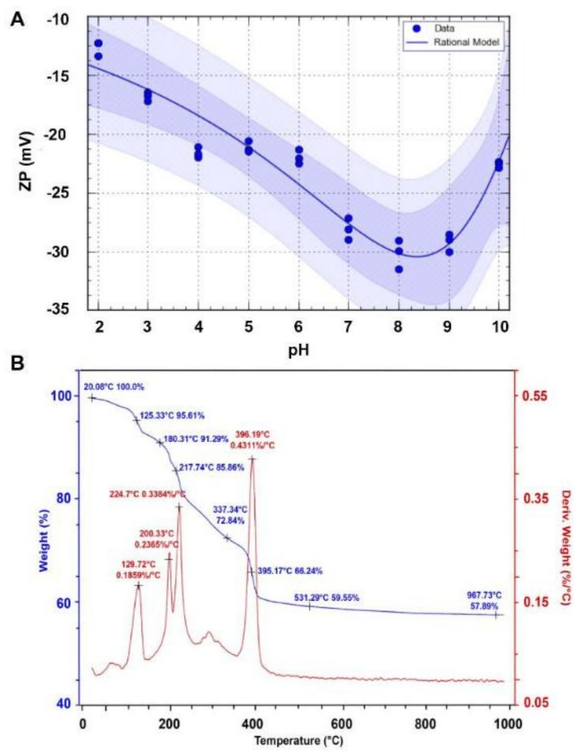

Figure 7. Zeta potential in the 2–10 pH range (**A**) and thermogravimetric TG/DTG curves (**B**) for biologically synthesized ZnO NCs.

Figure 7. Zeta potential in the 2–10 pH range (**A**) and thermogravimetric TG/DTG curves (**B**) for biologically synthesized ZnO NCs.

with the weight loss rate at 0.1859%/ C, is related to the removal of residual water. The second and third stages are similar to each other (200.33 C and 224.7 C, respectively) and appeared due to the elimination of coordinated water molecules [70,71]. The biggest change in the weight loss was observed from 217.74 C (85.86% of weight) to the 396.19 C (66.24% of weight)—it might be assigned to the decomposition step, including the removal of the organic deposit of nanocomposites and ending with the formation of ZnO [70–72]. No weight decline was observed at temperatures above 500 C. Vasile et al. [40] showed the good thermal stability of chemically synthesized ZnO nanocomposites to 200 C, whereas Basha et al. [73] described the green synthesis of nano-ZnO by using an alginate with thermal stability up to 160 C. Based on these data, it can be concluded that biosynthesis allowed the formation of slightly less thermostable ZnO NCs, which is closely related to values reached by our group.

3.2. Antimicrobial Activity of ZnO NCs

As shown in Table 1, the minimal inhibitory concentrations of biologically synthesized ZnO NCs were in the range of 86.25–172.5 g/mL. The maximum MIC value was found to be 172.5 g/mL for the E. coli ATCC 25922 and K. pneumonia ATCC BAA-1144 strains. On the other hand, S. aureus ATCC 11632 was susceptible to ZnO NC treatment at the lowest concentration (86.25 g/mL). The obtained nano-ZnO in our study did not present antibacterial e ects against P. aureginosa ATCC 15441 (Table 1). Furthermore, the experimental MIC values were in agreement with the CFU/mL values for each strain treated with nanocomposites. For the control sample of K. pneumonia, E. coli, P. aeruginosa and S. aureus, the CFU/mL values were 3.13 10^9, 2.81 10^9, 3.32 10^9 and 3.32 10^9, respectively. The ZnO NCs at 172.5 g/mL were su cient to inhibit the growth of K. pneumonia (7.41 10^8 CFU/mL) and E. coli (1.28 10^9). The MIC value for the S. aureus was found to be 86.25 g/mL and this concentration of nanocomposites reduced bacterial cells to 1.79 10^9 CFU/mL. The P. aureginosa strain was resistant to the ZnO NC treatment and the average CFU value was at the 3.16 10^9 level. As a positive control, ampicillin was applied—all bacterial strains except P. aureginosa were found to be sensitive to antibiotic treatment. Ampicillin at 10 g/mL concentration reduced the K. pneumonia, E. coli and S. aureus cell numbers to 2.30 10^9, 1.67 10^5 and 8.27 10^7, respectively. Colony forming units were also quantified for all bacterial cells and represented as percentage of viable cells in comparison to control sample (untreated culture) (Figure 8).

Table 1. Minimum inhibitory concentration (MIC) of the biologically synthesized ZnO NCs against tested microorganisms.

Tested Material	Klebsiella Pneumoniae	Escherichia Coli	Pseudomonas Aeruginosa	Staphylococcus Aureus
Access no.	ATCC BAA-1144	ATCC 25922	ATCC 15441	ATCC 11632
ZnO NCs	172.5 g/mL	172.5 g/mL	-	86.25 g/mL

In the present study, antibacterial properties of the ZnO NCs are slightly di erent to those described in previous reports related to nano-ZnO biological synthesis. According to [74], ZnO NPs produced by cyanobacterium Nostoc sp. [7] showed MIC values for S. aureus and E. coli of 64 g/mL and 2000 g/mL, respectively. Jayaseelan et al. [75] tested the intracellularly synthesized nano–ZnO by A. hydrophila against a few bacterial strains and they obtained the MIC in the 1.2–2.9 g/mL range. In our study, for S. aureus, the lowest concentration was 86.25 g/mL, whereas for the E. coli and K. pneumoniae strains, the concentration of ZnO NCs at 172.5 g/mL was enough to inhibit bacterial growth. Both S. aureus and E. coli have become a serious problem progressively observed not only in humans but also in veterinary medicine worldwide [22,76]. Although these bacteria strains are part of the commensal flora, they can also become opportunistic pathogens [77,78]. For instance, Staphylococcus aureus normally colonizes the nasal cavity. After breaking through its normal habitat, S. aureus is able to cause a number of infections, mainly skin or bloodstream infections and pneumonia. It has been widely observed that S. aureus has developed extraordinary resistance to almost all classes of antibiotics [21,23]. One of the bacterial strategies of protection from drugs and antibiotics is biofilm formation [79]. Strains tested in our study, such as S. aureus and P. aureginosa, have the propensity to form biofilms and then the proper antibiotic treatment is much more di cult [80]. One approach to controlling the production of these might be nanomaterials with antibacterial capabilities [81,82]. Some scientific reports have shown that nanoparticles have been e ectively applied to eliminate preformed biofilms or to stop their formation on the surfaces of medical equipment [83,84]. Eshed et al. [85] reported that ZnO NPs presented significant reduction in biofilm formation by Streptococcus mutants. Another work [86] indicated the ability of nano-ZnO to inhibit biofilms formed by vancomycin-resistant S. aureus. Therefore, the antibacterial activity of synthesized ZnO NCs in our study might be associated with their anti-biofilm behavior. However, our data also pointed out the absence of antibacterial activity against P. aeruginosa

ATCC—this strain is able to form a biofilm which protects the pathogen from host immune response and antimicrobial therapy [87]. Compared with Staphylococcus aureus, P. aeruginosa is a Gram( ) bacteria. **Table 1.** Minimum inhibitory concentration (MIC) of the biologically synthesized ZnO NCs against

Consequently,testedmicroorganismsduetothe .various cell wall structures, the antibacterial activity of zinc oxide NCs is

signif i ~~cantly di erent against Gram(+) and Gram( ) strains. The cell wall of Gram( ) spec~~ ies consist of lipopolysaccharides (LPS), lipoproteins and phospholipids, which act as a penetration barrier for nanostructures [88,89]. Taking this into consideration, it can be concluded that the entry of ZnO through the P. aureginosa cell wall is more di cult and thus they possess every antibacterial e ect.

Tested Material	***Klebsiella Pneumoniae***	***Escherichia Coli***	***Pseudomonas Aeruginosa***	***Staphylococcus Aureus***
NCs Access no.	ATCC BAA-1144	ATCC 25922	ATCC 15441	ATCC 11632
ZnO NCs	172.5 µg/mL	172.5 µg/mL	-	86.25 µg/mL

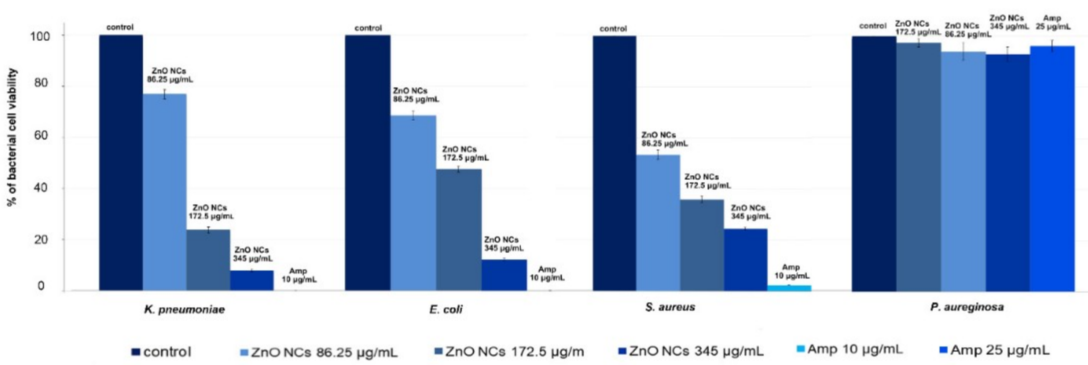

Figure 8. Quantification of bacterial cell viability (%) at di erent concentrations of ZnO NCs and ampicillin.

Figure 8. Quantification of bacterial cell viability (%) at different concentrations of ZnO NCs and ampicillin.

Another example of the opportunistic pathogens causing a broad spectrum of diseases and showing increasingly frequent acquisition of resistance to antibiotics is Klebsiella pneumoniae [20]. Hameed et al. [90] tested chemically synthesized ZnO NPs doped with Nd against K. pneumoniae—the inhibitory concentration was found to be 1000 g/mL. The work of Ansari et al. [91] pointed out that the minimum concentration of ZnO nanoparticles synthesized by the sol-gel method at the 100 g/mL inhibited the colony forming ability of K. pneumoniae. In comparison with the literature data, while

4. Conclusions

This study presents, for the first time, the use of *Lactobacillus paracasei* LPC20 strain isolated from whey as a new and efficient source for post-cultured ZnO nanocomposite synthesis. An minimal interdisciplinary approach, including a wide range of instrumental techniques, was used to evaluate structure, size, stability and organic deposits of the obtained nanocomposites. Scanning electron microscopy revealed the surface morphology and structure of biologically obtained nano-ZnO,

thetheMICtransmivaluessiforn Kelectron.pneumoniaemicroscopywerefounda todiffractionbemuch studylower. pointedTherefore,outit thecannotfrmationbeexcludedof the in the 7–9 pH range, with the average ZP value at the 29.15 1.05 mV level and thermal stability up to 130 C. Results of spectroscopic (photoluminescence and FT-IR) and spectrometric analysis pointed out the presence of organic deposits on the ZnO NCs' surfaces. According to the FT-IR data, the presence of signals corresponding to the deprotonated carboxyl groups of amino acids, mainly glutamic and aspartic acids, indicated their crucial participation in the biosynthesis process. Moreover, the FT-IR spectra also confirmed the presence of zinc oxide—the peak at the region between 500 and 600 cm^{1} was related to the Zn-O bond, which was in good agreement with the TEM/EDX and XRD data. The LDI-TOF MS/MS approach allowed identification of the amino acid sequences naturally present on the surfaces of ZnO NCs and an understanding of which types of amino acids might be linked to or interact with Zn^{2+}. The outcomes of our investigation additionally give an insight into our previous study and allow a clearer understanding of the mechanism of ZnO NC formation. Zinc is present in the form of an aqua complex and as an electron acceptor can interact with deprotonated carboxyl groups of bacterial enzymes or released metabolites. Based on the LDI-MS data and our previous work, the main role of amino acid functional groups (such as COO) in the subsequent aqua-hydroxo complex formation is strongly confirmed. Then, through further reaction, $[Zn(OH)_4]_2$ is transformed into ZnO. Furthermore, the fluorescence of biologically synthesized nanocomposites and the amplification of the signal in the presence of ZnO NCs, as well as the LDI analysis, create new application possibilities, e.g., as biosensors or matrixes in mass spectrometry.

Additionally, the biologically synthesized ZnO NCs exhibited good antimicrobial properties against clinically relevant Escherichia coli ATCC 25922, Staphylococcus aureus ATCC 11632 and Klebsiella pneumoniae ATCC BAA-1144. The MIC values obtained in our study are comparable to or even lower than those reported in the literature. Furthermore, the experimental MIC values were confirmed by the complementary colony forming units (CFU) assay. Accordingly, biologically synthesized ZnO NCs might be potentially used as a novel, easy-to-handle and antiseptic agent for external use, e.g., in bedsore treatment as a new type of skin path or in ointment formulations. Nevertheless, a further study regarding antibacterial activity against an expanded range of species by using other complementary techniques as well as cytotoxicity tests of ZnO NCs is needed.

Author Contributions: Conceptualization, B.B. and P.P.; methodology, A.K.-G. and V.R.-P.; software, V.R.-P.; validation, all authors; formal analysis, B.B. and P.P.; investigation, A.K.-G. and V.R.-P.; resources, P.P.; data curation, A.K.-G.; writing—original draft preparation, A.K.-G.; writing—review and editing, P.P. and V.R.-P.; visualization, V.R.-P. and A.K.-G.; supervision, P.P. and B.B.; project administration, P.P.; funding acquisition, P.P. All authors have read and agreed to the published version of the manuscript.

Funding: This research was funded by the National Science Centre under Opus 14 grant number 2017/27/B/ST4/02628 (2018–2021) and in part by the Torun´ Center of Excellence "Towards Personalized Medicine" operating under Excellence Initiative-Research University. Anna Król-Górniak obtained funds as part of financing a doctoral scholarship from the National Science Centre. Etiuda 7 No. 2019/32/T/ST4/00098 (2019–2020).

Conflicts of Interest: The authors declare no conflict of interest.

References

1. Keerthana, S.; Kumar, A. Potential risks and benefits of zinc oxide nanoparticles: A systematic review. Crit. Rev. Toxicol. **2020**, 50, 47–71. [CrossRef] [PubMed]
2. Król, A.; Pomastowski, P.; Rafinska,´ K.; Railean-Plugaru, V.; Buszewski, B. Zinc oxide nanoparticles: Synthesis, antiseptic activity and toxicity mechanism. Adv. Colloid Interface Sci. **2017**, 249, 37–52. [CrossRef] [PubMed]
3. Ogunyemi, S.O.; Abdallah, Y.; Zhang, M.; Fouad, H.; Hong, X.; Ibrahim, E.; Masum, M.M.I.; Hossain, A.; Mo, J.; Li, B. Green synthesis of zinc oxide nanoparticles using di erent plant extracts and their antibacterial activity against Xanthomonas oryzae pv. oryzae. Artif. Cells Nanomed. Biotechnol. **2019**, 47, 341–352. [CrossRef] [PubMed]
4. Kalpana, V.N.; Kataru, B.A.S.; Sravani, N.; Vigneshwari, T.; Panneerselvam, A.; Devi Rajeswari, V. Biosynthesis of zinc oxide nanoparticles using culture filtrates of Aspergillus niger: Antimicrobial textiles and dye degradation studies. OpenNano **2018**, 3, 48–55. [CrossRef]
5. Król, A.; Railean-Plugaru, V.; Pomastowski, P.; Buszewski, B. Phytochemical investigation of Medicago sativa L. extract and its potential as a safe source for the synthesis of ZnO nanoparticles: The proposed mechanism of formation and antimicrobial activity. Phytochem. Lett. **2019**, 31, 170–180. [CrossRef]
6. Salvadori, M.R.; Ando, R.A.; Oller Nascimento, C.A.; Corrêa, B. Extra and Intracellular Synthesis of Nickel Oxide Nanoparticles Mediated by Dead Fungal Biomass. PLoS ONE **2015**, 10, e0129799. [CrossRef]
7. Ovais, M.; Khalil, A.; Ayaz, M.; Ahmad, I.; Nethi, S.; Mukherjee, S. Biosynthesis of Metal Nanoparticles via Microbial Enzymes: A Mechanistic Approach. Int. J. Mol. Sci. **2018**, 19, 4100. [CrossRef]
8. Grasso, G.; Zane, D.; Dragone, R. Microbial nanotechnology: Challenges and prospects for green biocatalytic synthesis of nanoscale materials for sensoristic and biomedical applications. Nanomaterials **2020**, 10, 11. [CrossRef]
9. Das, V.L.; Thomas, R.; Varghese, R.T.; Soniya, E.V.; Mathew, J.; Radhakrishnan, E.K. Extracellular synthesis of silver nanoparticles by the Bacillus strain CS 11 isolated from industrialized area. 3 Biotech **2014**, 4, 121–126. [CrossRef]
10. Railean-Plugaru, V.; Pomastowski, P.P.; Meller, K.; Złoch, M.; Rafinska,´ K.; Buszewski, B. Lactococcus lactis as a safe and inexpensive source of bioactive silver composites. Appl. Microbiol. Biotechnol. **2017**, 101, 7141–7153. [CrossRef]
11. Kundu, D.; Hazra, C.; Chatterjee, A.; Chaudhari, A.; Mishra, S. Extracellular biosynthesis of zinc oxide nanoparticles using Rhodococcus pyridinivorans NT2: Multifunctional textile finishing, biosafety evaluation and in vitro drug delivery in colon carcinoma. J. Photochem. Photobiol. B Biol. **2014**, 140, 194–204. [CrossRef] [PubMed]
12. Gupta, R.; Srivastava, S. Antifungal e ect of antimicrobial peptides (AMPs LR14) derived from Lactobacillus plantarum strain LR/14 and their applications in prevention of grain spoilage. Food Microbiol. **2014**, 42, 1–7. [CrossRef] [PubMed]
13. Ren, D.; Zhu, J.; Gong, S.; Liu, H.; Yu, H. Antimicrobial Characteristics of Lactic Acid Bacteria Isolated from Homemade Fermented Foods. Biomed Res. Int. **2018**, 2018, 5416725. [CrossRef] [PubMed]
14. Selvarajan, E.; Mohanasrinivasan, V. Biosynthesis and characterization of ZnO nanoparticles using Lactobacillus plantarum VITES07. Mater. Lett. **2013**, 112, 180–182. [CrossRef]

15. Al-Zahrani, H.A.A.; El-Waseif, A.A.; El-Ghwas, D.E. Biosynthesis and evaluation of TiO 2 and ZnO nanoparticles from in vitro stimulation of Lactobacillus johnsonii. J. Innov. Pharm. Biol. Sci. **2018**, 5, 16–20.
16. Mohd Yusof, H.; Mohamad, R.; Zaidan, U.H.; Rahman, N.A. Sustainable microbial cell nanofactory for zinc oxide nanoparticles production by zinc-tolerant probiotic Lactobacillus plantarum strain TA4. Microb. Cell Fact. **2020**, 19, 10. [CrossRef]
17. Gaynes, R. The discovery of penicillin—New insights after more than 75 years of clinical use. Emerg. Infect. Dis. **2017**, 23, 849–853. [CrossRef]
18. Li, B.; Webster, T.J. Bacteria antibiotic resistance: New challenges and opportunities for implant-associated orthopedic infections. J. Orthop. Res. **2018**, 36, 22–32. [CrossRef]
19. Peterson, E.; Kaur, P. Antibiotic resistance mechanisms in bacteria: Relationships between resistance determinants of antibiotic producers, environmental bacteria, and clinical pathogens. Front. Microbiol. **2018**, 9. [CrossRef]
20. E ah, C.Y.; Sun, T.; Liu, S.; Wu, Y. Klebsiella pneumoniae: An increasing threat to public health. Ann. Clin. Microbiol. Antimicrob. **2020**, 19, 1. [CrossRef]
21. Lowy, F.D. Antimicrobial resistance: The example of Staphylococcus aureus. J. Clin. Investig. **2003**, 111, 1265–1273. [CrossRef] [PubMed]
22. Poirel, L.; Madec, J.-Y.; Lupo, A.; Schink, A.-K.; Kie er, N.; Nordmann, P.; Schwarz, S. Antimicrobial Resistance in Escherichia coli. In Antimicrobial Resistance in Bacteria from Livestock and Companion Animals; Wiley: Hoboken, NJ, USA, 2018; Volume 6, pp. 289–316.
23. Chambers, H.F.; DeLeo, F.R. Waves of resistance: Staphylococcus aureus in the antibiotic era. Nat. Rev. Microbiol. **2009**, 7, 629–641. [CrossRef] [PubMed]
24. De Wit, J.N. Nutritional and Functional Characteristics of Whey Proteins in Food Products. J. Dairy Sci. **1998**, 81, 597–608. [CrossRef]
25. Rodzik, A.; Pomastowski, P.; Sagandykova, G.N.; Buszewski, B. Interactions of whey proteins with metal ions. Int. J. Mol. Sci. **2020**, 21, 2156. [CrossRef] [PubMed]
26. Pomastowski, P.; Złoch, M.; Rodzik, A.; Ligor, M.; Kostrzewa, M.; Buszewski, B. Analysis of bacteria associated with honeys of di erent geographical and botanical origin using two di erent identification approaches: MALDI-TOF MS and 16S rDNA PCR technique. PLoS ONE **2019**, 14, e0217078. [CrossRef]
27. Milanowski, M.; Pomastowski, P.; Railean-Plugaru, V.; Rafinska,´ K.; Ligor, T.; Buszewski, B. Biosorption of silver cations onto Lactococcus lactis and Lactobacillus casei isolated from dairy products. PLoS ONE **2017**, 12, e0174521. [CrossRef]
28. Muniz, F.T.L.; Miranda, M.A.R.; Morilla Dos Santos, C.; Sasaki, J.M. The Scherrer equation and the dynamical theory of X-ray di raction. Acta Crystallogr. Sect. A Found. Adv. **2016**, 72, 385–390. [CrossRef]
29. Railean-Plugaru, V.; Pomastowski, P.; Kowalkowski, T.; Sprynskyy, M.; Buszewski, B. Physicochemical study of natural fractionated biocolloid by asymmetric flow field-flow fractionation in tandem with various complementary techniques using biologically synthesized silver nanocomposites. Anal. Bioanal. Chem. **2018**, 410, 2837–2847. [CrossRef]
30. Suckau, D.; Resemann, A.; Schuerenberg, M.; Hufnagel, P.; Franzen, J.; Holle, A. A novel MALDI LIFT-TOF/TOF mass spectrometer for proteomics. Anal. Bioanal. Chem. **2003**, 376, 952–965. [CrossRef]
31. Elshikh, M.; Ahmed, S.; Funston, S.; Dunlop, P.; McGaw, M.; Marchant, R.; Banat, I.M. Resazurin-based 96-well plate microdilution method for the determination of minimum inhibitory concentration of biosurfactants. Biotechnol. Lett. **2016**, 38, 1015–1019. [CrossRef]

32. Buszewski, B.; Railean-Plugaru, V.; Pomastowski, P.; Rafinska,´ K.; Szultka-Mlynska, M.; Golinska, P.; Wypij, M.; Laskowski, D.; Dahm, H. Antimicrobial activity of biosilver nanoparticles produced by a novel Streptacidiphilus durhamensis strain. J. Microbiol. Immunol. Infect. **2018**, 51, 45–54. [CrossRef] [PubMed]
33. Nangia, Y.; Wangoo, N.; Goyal, N.; Shekhawat, G.; Suri, C.R. A novel bacterial isolate Stenotrophomonas maltophilia as living factory for synthesis of gold nanoparticles. Microb. Cell Fact. **2009**, 8, 39. [CrossRef] [PubMed]
34. Taran, M.; Rad, M.; Alavi, M. Biosynthesis of TiO2 and ZnO nanoparticles by Halomonas elongata IBRC-M 10214 in di erent conditions of medium. BioImpacts **2018**, 8, 81–89. [CrossRef] [PubMed]
35. Zheng, J.; Nagashima, K.; Parmiter, D.; de la Cruz, J.; Patri, A.K. SEM X-ray microanalysis of nanoparticles present in tissue or cultured cell thin sections. Methods Mol. Biol. **2011**, 697, 93–99. [CrossRef] [PubMed]
36. Narayana, A.; Bhat, S.A.; Fathima, A.; Lokesh, S.V.; Surya, S.G.; Yelamaggad, C.V. Green and low-cost synthesis of zinc oxide nanoparticles and their application in transistor-based carbon monoxide sensing. RSC Adv. **2020**, 10, 13532–13542. [CrossRef]
37. Gavrilenko, E.A.; Goncharova, D.A.; Lapin, I.N.; Nemoykina, A.L.; Svetlichnyi, V.A.; Aljulaih, A.A.; Mintcheva, N.; Kulinich, S.A. Comparative study of physicochemical and antibacterial properties of zno nanoparticles prepared by laser ablation of zn target in water and air. Materials **2019**, 12, 186. [CrossRef]
38. Yang, Z.X.; Zhong, W.; Au, C.; Wang, J.Y.; Du, Y.W. An environment-benign solvothermal method for the synthesis of flower-like hierarchical nickel and zinc compounds and their transformation to nanoporous NiO and ZnO. CrystEngComm **2011**, 13, 1831–1837. [CrossRef]
39. Wahab, R.; Ansari, S.G.; Kim, Y.S.; Song, M.; Shin, H.S. The role of pH variation on the growth of zinc oxide nanostructures. Appl. Surf. Sci. **2009**, 255, 4891–4896. [CrossRef]
40. Vasile, O.R.; Serdaru, I.; Andronescu, E.; Tru¸sc@, R.; Surdu, V.A.; Oprea, O.; Ilie, A.; Vasile, B.S¸. Influence of the size and the morphology of ZnO nanoparticles on cell viability. Comptes Rendus Chim. **2015**, 18, 1335–1343. [CrossRef]
41. Vasile, O.R.; Andronescu, E.; Ghitulica, C.; Vasile, B.S.; Oprea, O.; Vasile, E.; Trusca, R. Synthesis and characterization of nanostructured zinc oxide particles synthesized by the pyrosol method. J. Nanopart. Res. **2012**, 14, 1–13. [CrossRef]
42. Nicolardi, S.; Palmblad, M.; Dalebout, H.; Bladergroen, M.; Tollenaar, R.A.E.M.; Deelder, A.M.; van der Burgt, Y.E.M. Quality control based on isotopic distributions for high-throughput MALDI-TOF and MALDI-FTICR serum peptide profiling. J. Am. Soc. Mass Spectrom. **2010**, 21, 1515–1525. [CrossRef] [PubMed]
43. Polfer, N.C.; Oomens, J.; Moore, D.T.; Von Helden, G.; Meijer, G.; Dunbar, R.C. Infrared spectroscopy of phenylalanine Ag(I) and Zn(II) complexes in the gas phase. J. Am. Chem. Soc. **2006**, 128, 517–525. [CrossRef] [PubMed]
44. Hernández, B.; Pflüger, F.; Adenier, A.; Kruglik, S.G.; Ghomi, M. Vibrational analysis of amino acids and short peptides in hydrated media. VIII. Amino acids with aromatic side chains: L-phenylalanine, l-tyrosine, and l-tryptophan. J. Phys. Chem. B **2010**, 114, 15319–15330. [CrossRef]
45. Nˇemec, I.; Miˇcka, Z. FTIR and FT Raman study of L-leucine addition compound with nitric acid. J. Mol. Struct. **1999**, 482–483, 23–28.

46. Kalsi, P.S. Spectroscopy of Organic Compounds; New Age International: New Delhi, India, 2006; ISBN 8122415431.
47. Nara, M.; Torii, H.; Tasumi, M. Correlation between the vibrational frequencies of the carboxylate group and the types of its coordination to a metal ion: An ab initio molecular orbital study. J. Phys. Chem. **1996**, 100, 19812–19817. [CrossRef]
48. Fischer, G.; Cao, X.; Cox, N.; Francis, M. The FT-IR spectra of glycine and glycylglycine zwitterions isolated in alkali halide matrices. Chem. Phys. **2005**, 313, 39–49. [CrossRef]
49. Parker, S.F. Assignment of the vibrational spectrum of l-cysteine. Chem. Phys. **2013**, 424, 75–79. [CrossRef]
50. Mohamed, M.E.; Mohammed, A.M.A. Experimental and Computational Vibration Study of Amino Acids.
Int. Lett. Chem. Phys. Astron. **2013**, 15, 1–17. [CrossRef]
51. Barth, A. Infrared spectroscopy of proteins. Biochim. Biophys. Acta—Bioenerg. **2007**, 1767, 1073–1101. [CrossRef]
52. Vodnar, D.C.; Paucean, A.; Dulf, F.V.; Socaciu, C. HPLC characterization of lactic acid formation and FTIR fingerprint of probiotic bacteria during fermentation processes. Not. Bot. Horti Agrobot. Cluj-Napoca **2010**, 38, 109–113. [CrossRef]
53. Keyes, B.M.; Gedvilas, L.M.; Li, X.; Coutts, T.J. Infrared spectroscopy of polycrystalline ZnO and ZnO:N thin films. J. Cryst. Growth **2005**, 281, 297–302. [CrossRef]
54. Król, A.; Railean-Plugaru, V.; Pomastowski, P.; Złoch, M.; Buszewski, B. Mechanism study of intracellular zinc oxide nanocomposites formation. Colloids Surfaces A Physicochem. Eng. Asp. **2018**, 553, 349–358. [CrossRef]
55. Kr˛ezel,˙ A.; Maret, W. The biological inorganic chemistry of zinc ions. Arch. Biochem. Biophys. **2016**, 611, 3–19. [CrossRef] [PubMed]
56. Rulíšek, L.; Vondrášek, J. Coordination geometries of selected transition metal ions (Co^{2+}, Ni^{2+}, Cu^{2+}, Zn^{2+}, Cd^{2+}, and Hg^{2+}) in metalloproteins. J. Inorg. Biochem. **1998**, 71, 115–127. [CrossRef]
57. Tang, N.; Skibsted, L.H. Zinc bioavailability from whey. Enthalpy-entropy compensation in protein binding. Food Res. Int. **2016**, 89, 749–755. [CrossRef]
58. Pomastowski, P.; Sprynskyy, M.; Buszewski, B. The study of zinc ions binding to casein. Colloids Surfaces B Biointerfaces **2014**, 120, 21–27. [CrossRef]
59. Srikant, V.; Clarke, D.R. On the optical band gap of zinc oxide. J. Appl. Phys. **1998**, 83, 5447–5451. [CrossRef]
60. Szmacinski, H.; Ray, K.; Lakowicz, J.R. E ect of plasmonic nanostructures and nanofilms on fluorescence resonance energy transfer. J. Biophotonics **2009**, 2, 243–252. [CrossRef]
61. Jana, J.; Ganguly, M.; Pal, T. Enlightening surface plasmon resonance e ect of metal nanoparticles for practical spectroscopic application. RSC Adv. **2016**, 6, 86174–86211. [CrossRef]
62. Bah, A.; Lim, K.Y.; Wei, F.; Khursheed, A.; Sow, C.H. Fluorescence Invigoration in Carbon-Incorporated Zinc Oxide Nanowires from Passage of Field Emission Electrons. Sci. Rep. **2019**, 9, 1–12. [CrossRef]
63. Das, R.; Phadke, P.; Khichar, N.; Chawla, S. Plasmonic enhancement of blue fluorescence in ZnO nanoparticles.
Superlattices Microstruct. **2015**, 85, 658–663. [CrossRef]
64. Kang, M.-J.; Pyun, J.-C.; Lee, J.-C.; Choi, Y.-J.; Park, J.-H.; Park, J.-G.; Lee, J.-G.; Choi, H.-J. Nanowire-assisted laser desorption and ionization mass spectrometry for quantitative analysis of small molecules. Rapid Commun. Mass Spectrom. **2005**, 19, 3166–3170. [CrossRef]

65. Pomastowski, P.; Buszewski, B. Complementarity of matrix-and nanostructure-assisted laser desorption/ionization approaches. Nanomaterials **2019**, 9, 260. [CrossRef] [PubMed]
66. Watanabe, T.; Kawasaki, H.; Yonezawa, T.; Arakawa, R. Surface-assisted laser desorption/ionization mass spectrometry (SALDI-MS) of low molecular weight organic compounds and synthetic polymers using zinc oxide (ZnO) nanoparticles. J. Mass Spectrom. **2008**, 43, 1063–1071. [CrossRef]
67. Degen, A.; Kosec, M. E ect of pH and impurities on the surface charge of zinc oxide in aqueous solution. J. Eur. Ceram. Soc. **2000**, 20, 667–673. [CrossRef]
68. Fatehah, M.O.; Aziz, H.A.; Stoll, S. Stability of ZnO Nanoparticles in Solution. Influence of pH, Dissolution, Aggregation and Disaggregation E ects. J. Colloid Sci. Biotechnol. **2014**, 3, 75–84. [CrossRef]
69. Reichle, R.A.; McCurdy, K.G.; Hepler, L.G. Zinc Hydroxide: Solubility Product and Hydroxy-complex Stability Constants from 12.5–75 C. Can. J. Chem. **1975**, 53, 3841–3845. [CrossRef]
70. Prochowicz, D.; Sokołowski, K.; Lewinski,´ J. Zinc hydroxides and oxides supported by organic ligands: Synthesis and structural diversity. Coord. Chem. Rev. **2014**, 270–271, 112–126. [CrossRef]
71. Siddiqui, K.A.; Bharati, A.K.; Lama, P. Zinc-orotate coordination polymer: Synthesis, thermogravimetric analysis and luminescence properties. SN Appl. Sci. **2020**, 2, 1–11. [CrossRef]
72. Sujamol, M.S.; Athira, C.J.; Sindhu, Y.; Mohanan, K. Synthesis, spectroscopic characterization, electrochemical behaviour and thermal decomposition studies of some transition metal complexes with an azo derivative. Spectrochim. Acta-Part A Mol. Biomol. Spectrosc. **2010**, 75, 106–112. [CrossRef]
73. Basha, S.K.; Lakshmi, K.V.; Kumari, V.S. Ammonia sensor and antibacterial activities of green zinc oxide nanoparticles. Sens. Bio-Sens. Res. **2016**, 10, 34–40. [CrossRef]